Journal of Solid State Chemistry 183 (2010) 1925–1934

Contents lists available at ScienceDirect

Journal of Solid State Chemistry

journal homepage: www.elsevier.com/locate/jssc

Antimony and silicon environments in antimony silicate glasses

M. Mee [a], B.C. Davies [a], R.G. Orman [a], M.F. Thomas [b], D. Holland [a,*]

[a] Department of Physics, University of Warwick, Coventry CV4 7AL, UK
[b] Department of Physics, University of Liverpool, Liverpool L69 3BX, UK

ARTICLE INFO

Article history:
Received 24 March 2010
Received in revised form
16 June 2010
Accepted 17 June 2010
Available online 26 June 2010

Keywords:
Antimony silicate
Glass
^{29}Si NMR
^{121}Sb Mössbauer spectroscopy

ABSTRACT

Antimony silicate glasses, of general formula $xSb_2O_3 \cdot (1-x)SiO_2$ ($0.1 \le x \le 0.78$), have been prepared by melt-quenching and their structures studied using ^{29}Si MAS NMR spectroscopy, ^{121}Sb Mössbauer spectroscopy and Raman spectroscopy. Oxidation during melting gives rise to Sb^{5+} in concentrations, which increase linearly with x to give a value of ~10% when $x=0.78$. ^{121}Sb Mössbauer spectra show Mössbauer shifts and quadrupole splittings consistent with Sb^{3+} in a [:SbO_3] trigonal pyramid, similar to that in crystalline Sb_2O_3. A broad band in the Raman spectrum at ~410 cm^{-1} is due to the vibrations of such a unit. The dependence of the silicon Q^n speciation on x can be interpreted by the formation of Sb–O–Sb links possibly to form rings of 4 [:SbO_3] units such as are found in valentinite.

1. Introduction

Antimony oxide, Sb_2O_3, contains the lone-pair cation Sb^{3+}, which has the electron configuration $4d^{10}5s^2$. The non-bonding $5s^2$ "lone-pair" of electrons can remain spherically symmetric or the $5s^2$ can hybridise with $5p$ (and even $5d$) to produce a lone-pair which is positioned to one side of the cation to an extent which is determined by the p_z character of the hybridisation. This situation is common in the lower oxidation state of several heavy metals (Sn^{2+}, Te^{4+}, Tl^{+}, Pb^{2+}, Bi^{3+}). We have been examining the environments of such cations in glass networks, partly to see if the lack of long-range order has any effect on the geometry of the cation environment but also because some of these oxides can be the major and indeed sole components of glasses. The asymmetric distribution of polarisable charge can lead to interesting non-linear optical behaviour in materials containing such cations and glasses containing Sb_2O_3 have been investigated as laser hosts and waveguides because of their large, third-order, non-linear optical coefficients [1,2]. The mixed-valence capacity of antimony has also led to the study of the conduction properties of the silicate glasses [3,4].

Zachariasen [5] predicted that Sb_2O_3 should itself be a glass former although, until recently [6], Sb_2O_3 glass could only be prepared with the inclusion (deliberate or accidental) of a few percent of a second oxide [7–11] or anion [12]. There have been various reports of antimony borate [11,13–17], silicate [18], germanate [18] and arsenate glass systems [18], indicating that glass formation is possible over most of the composition range. Bednarik and Neely [7,8] prepared v-Sb_2O_3 in a quartz ampoule and the resulting product, when they used spectroscopically pure Sb_2O_3 as a starting material, contained 2.4 mole% SiO_2. Terashima et al. [11] produced Sb_2O_3 by a similar route and inductively coupled plasma analysis indicated the presence of 2 mole% SiO_2, which was also evident in the infra-red spectrum from the material. Datta et al. [4] used a sol–gel route to produce $xSb_2O_3 \cdot (1-x)SiO_2$ glasses with $x=0.07$ and 0.23, which they used for AC resistivity measurements. Their purpose in using the sol–gel method was to keep the fabrication temperature down so as to increase the proportion of the higher oxidation state, Sb^{5+}. Ellison and Sen [18] performed Sb K-edge extended X-ray absorption fine-structure spectroscopic (EXAFS) studies on $xSb_2O_3 \cdot (1-x)SiO_2$ conventionally melted glasses with analysed compositions $x=0.12$–0.81. They obtained a Sb–O coordination number of 3 and Sb–O distances in the range 1.945–1.970 Å for these glasses and also for similar compositions where B_2O_3, P_2O_5, GeO_2 or As_2O_3 was the network former instead of SiO_2. This is consistent with Sb having a trigonal pyramidal arrangement of oxygen atoms to one side of the cation, with the lone-pair of electrons to the other ([:SbO_3]). This can also be considered as a pseudo-tetrahedral unit with one vertex occupied by the lone-pair. There is more extensive literature on the antimony borate glass system [11,13–17] and the results from the various techniques employed in those studies are in agreement with the description of the local environment of Sb^{3+} published by Ellison and Sen [18].

Herein we report a multi-technique study of the structure and properties of antimony silicate glasses and describe the local environments of antimony and silicon.

* Corresponding author.
E-mail address: d.holland@warwick.ac.uk (D. Holland).

0022-4596/$ - see front matter © 2010 Elsevier Inc. All rights reserved.
doi:10.1016/j.jssc.2010.06.014

2. Experimental

2.1. Sample preparation

Glass samples of nominal composition $x\mathrm{Sb_2O_3}\cdot(1-x)\mathrm{SiO_2}$ ($x=0.1$, 0.2, 0.3, 0.4, 0.5, 0.55, 0.6, 0.7, 0.8) were produced from powdered Wacomsil quartz (>99.9% purity) and Sb_2O_3 (99.6%) in batches of 25–50 g. Powders were mixed and heated in silica crucibles (to avoid introduction of other elements) with silica or alumina lids. The temperatures used to melt the glasses (Table 1) depended on the SiO_2 content, which raises the melting point considerably. They were heated from room temperature to the required melting temperature at 10 °C/min and then held for ~15 min to achieve mixing before being cooled, either by splat quenching or by cooling in the crucible at room temperature (Table 1). Samples were stored in a desiccator until required for analysis.

2.2. Sample characterisation

2.2.1. X-ray diffraction (XRD)

X-ray diffraction was used to check the samples for amorphousness and also to identify any crystal phases formed. Diffraction was performed on a Bruker D5005 diffractometer with Cu $K\alpha$ radiation at 40 kV–30 mA with slit size 1° and a 12 mm footprint on sample. Scans were run over 15–60° (2θ) with 0.02° (2θ) increments and acquisition time 3–25 s per increment depending on signal/noise levels.

2.2.2. Energy dispersive X-ray analysis (EDX)

A JEOL 6100 Scanning Electron Microscope was used with 10 kV accelerating voltage for EDX analysis. Powdered samples were mounted on carbon sticky pads on aluminium stubs and three measurements were taken on different areas of each sample in order to estimate the extent of any inhomogeneity.

2.2.3. Mössbauer spectroscopy (MS)

Mössbauer spectroscopy was performed on powdered samples, at 77 K, using a room temperature ^{121}Sb source ($Ca^{121m}SnO_3$) with constant acceleration drive. The velocity scale was calibrated with a ^{57}Fe Mössbauer absorber and a ^{57}Co source. The detector was a liquid nitrogen-cooled, intrinsic germanium, solid-state detector and the temperature of the glass sample was controlled using a continuous-flow liquid helium cryostat. The velocity scale was subsequently converted to the standard InSb reference by adding 8.6 mm s^{-1}. The similarity of the recoil-free fractions (f-factors) at 77 K for Sb^{3+} and Sb^{5+} was checked using a sample of cervantite ($Sb_2O_4 \equiv Sb^{3+}Sb^{5+}O_4$), known to contain equal proportions of Sb^{3+} and Sb^{5+}, and the integrated areas of the two peaks were found to be equal. Assuming that the environments, and hence Debye temperatures, of the species in Sb_2O_4 are similar to those in the glasses studied, we can regard the integrated areas of the peaks in the spectra from the glasses as being proportional to the populations of the two oxidation states. However, it should be noted that variable temperature measurements which we conducted on antimony borate glasses showed that an ~20% increase in Sb(III) relative intensity can occur on cooling from 77 to 10 K [unpublished].

Table 1
Summary of glass samples produced, composition and production methods.

x-Sb_2O_3 mole fraction			Batch size (g)	Max temp (°C) ± 20
Nominal		EDX analysis ± 0.025		
0.1	C	0.10	25	1600
0.2	C	0.23	25	1400
0.3	C	0.31	25	1400
0.4	C	0.38	25	1400
0.5	C	0.45	25	1400
0.55	SQ	0.60	35	1150
0.6	C	0.44	25	1400
0.6[a]	C	0.42	25	1400
0.6	SQ	0.66	50	1150
0.7	SQ	0.70	35	1150
0.8	SQ	0.78	35	1150

Cooling method "C" – cooled in crucible, "SQ" – splat-quenched.

[a] Sample held at temperature for a long period to determine effect on Sb oxidation state.

2.2.4. Density

Densities (ρ) were determined using a Micromeritics AccuPyc 1330 pycnometer with helium as the displacement fluid. Molar volumes (V_M) were then calculated using $V_M=\rho/M$, where M is the molar mass according to the unit formula $x\mathrm{Sb_2O_3}\cdot(1-x)\mathrm{SiO_2}$.

2.2.5. Raman spectroscopy (RS)

Raman spectroscopy was performed using a Renishaw Invia Raman Spectrometer equipped with a 20 mW laser source of wavelength 514 nm. Measurements were taken with 10 mW incident laser power at 50× magnification at room temperature over a wavenumber range of 100–3200 cm^{-1}, taking 60 scans at 10 s per acquisition, at 100% power. In addition to the glasses, measurements were also performed on crystalline Sb_2O_3 polymorphs, senarmontite (commercial) and valentinite (produced by mechanical milling [19]).

2.2.6. Differential thermal analysis (DTA)

Differential thermal analysis was performed using a Stanton-Redcroft DTA 673-4 with a heating/cooling rate of 10 °C min^{-1} over the temperature range 30–1450 °C. Powdered samples, of typical mass 160 mg, were contained in the 90%Pt/10%Rh sample crucible and the equivalent mass of quartz was used as the reference. Data were obtained at ambient pressure in either static air or argon flowing at a rate of 250 ml min^{-1}.

2.2.7. ^{29}Si magic-angle-spinning (MAS) nuclear magnetic resonance (NMR)

^{29}Si MAS NMR spectra were acquired at 8.5 T using a CMX360 Infinity spectrometer at 71.54 MHz. Samples were held in a 6 mm zirconia rotor and an MAS frequency of 5.5–6 kHz employed. A pulse width of 2 μs (30° tip angle), a pre-acquisition delay of 30 μs and pulse delay of 60 s were used to obtain quantitative spectra. Approximately 1000–2000 acquisitions were taken to obtain sufficient S/N for spectra to be analysed by peak fitting and an exponential line broadening of 150 Hz was applied prior to Fourier transform.

3. Results

3.1. Glass formation

Most compositions formed yellow glasses, with the colour intensity increasing with Sb_2O_3 content, and the XRD patterns were typical of an amorphous structure. The $x=0.1$ nominal composition did not melt fully and crystalline quartz was detected in the sample by XRD. Some macroscopic (several mm^3) phase separation was observed in the nominal $x=0.3$ glass, which had been cooled in the crucible, giving regions of lighter and darker yellow. The comparatively slow cooling of this sample had possibly encouraged this separation. The regions were easily mechanically separated from

each other and subsequent measurements were conducted on the lighter yellow phase, which was determined by EDX to be closest in composition to the nominal.

3.2. EDX analysis

The compositions of the glasses, as determined by EDX analysis, are summarised in Table 1 and plotted against the nominal compositions in Fig. 1 which shows the problems associated with melting small quantities of batch, at high temperature, and then cooling relatively slowly. The EDX analysed compositions of such glasses, for nominal $x > 0.4$, are all equivalent to $x \sim 0.45$ and indicate that either antimony oxide loss has occurred (by volatilisation) or that excessive reaction with the crucible material (silica) has taken place. Remaking the glasses with larger batch size, lower melting temperature and using splat quenching reduced these problems. All the quantitative EDX measurements here have an associated error of $\pm 2\%$; however, some samples showed nearly $\pm 2.5\%$ deviation from the mean between different positions on the sample and therefore this value is used as an estimate of the overall error in composition in subsequent data processing.

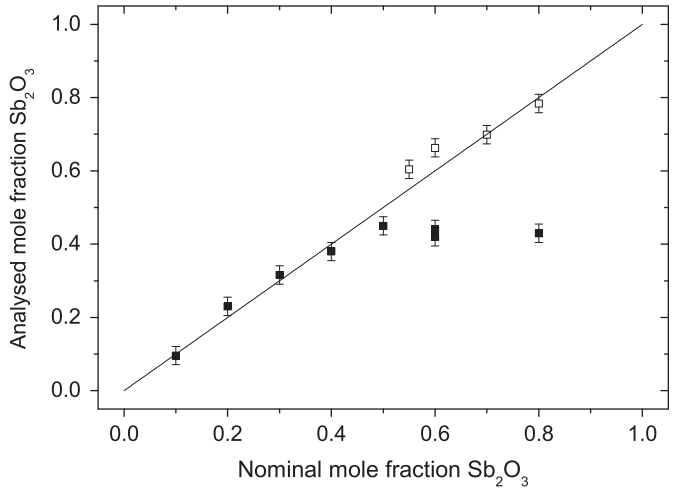

Fig. 1. Comparison of nominal and EDX analysed compositions of $x Sb_2O_3 \cdot (1-x)$-SiO_2 glasses: (■) small batch, high temperature and (□) large batch, low temperature (see Table 1 for details). The solid line is $y=x$.

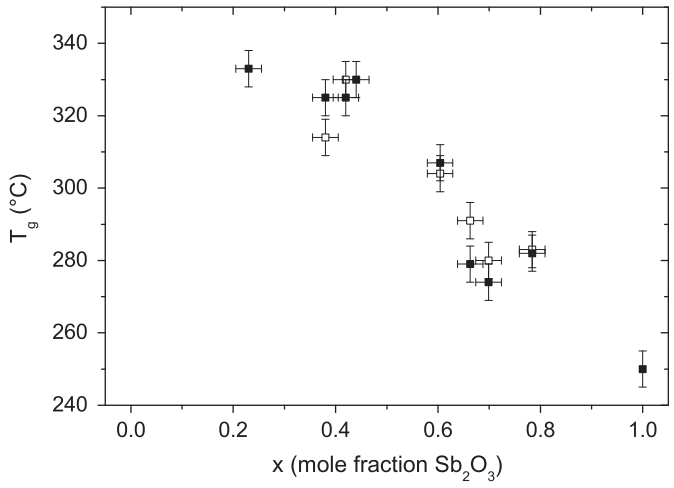

Fig. 2. Change in glass transition temperature, T_g, as a function of analysed composition, x, of $x Sb_2O_3 \cdot (1-x) SiO_2$ glasses: (■) air and (□) argon.

3.3. Thermal analysis

DTA traces showed a single glass transition temperature, T_g. At higher temperatures, a general exothermic rise in the background occurred due to oxidation of those samples run in air. Fig. 2 summarises the values of T_g for the different glass compositions studied here. There are significant and non-systematic differences between the T_g values obtained for DTA samples run in air and in argon but the general trend is for a decrease in T_g with increase in x until the value for v-Sb_2O_3 [6] is reached at 250 °C.

3.4. Density and molar volume

Densities are plotted as a function of mole fraction of Sb_2O_3 in Fig. 3(a) and the corresponding molar volumes are plotted in Fig. 3(b). Also plotted (solid lines) are the theoretical values for both ρ and V_M, calculated using a weighted combination of the

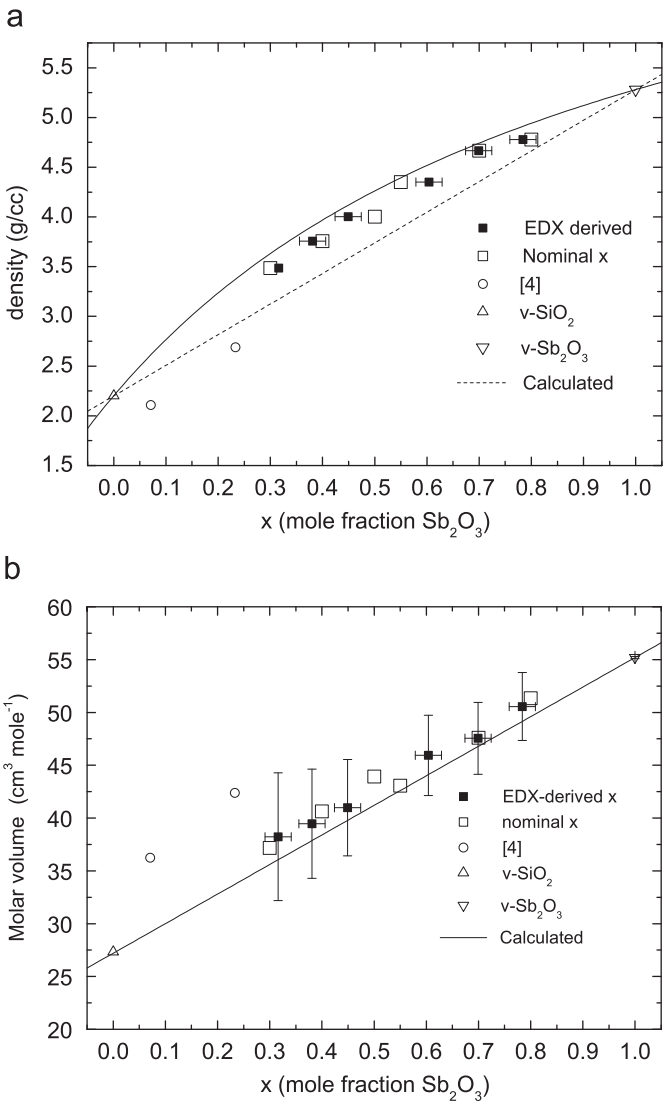

Fig. 3. (a) Density as a function of nominal (■) and analysed (□) composition, x, of $x Sb_2O_3 \cdot (1-x) SiO_2$ glasses, compared with that predicted by simple linear combination (dotted line) and using the formula $\rho = (x^* M_{Sb_2O_3} + (1-x)^* M_{SiO_2})/V_M$ (solid line) where $V_M = x^* V_{M(Sb_2O_3)} + (1-x)^* V_{M(SiO_2)}$. The error bars for density are smaller than the symbols. (b) Molar volume as a function of nominal (■) and analysed (□) composition, x, of $x Sb_2O_3 \cdot (1-x) SiO_2$ glasses, compared with that predicted by simple linear combination (line) $V_M = x^* V_M(Sb_2O_3) + (1-x)^* V_M(SiO_2)$.

values for the end members

$$V_M = x^*V_M(Sb_2O_3)+(1-x)^*V_M(SiO_2)$$

and

$$\rho = (x^*M_{Sb_2O_3}+(1-x)^*M_{SiO_2})/V_M,$$

where $M_{Sb_2O_3}$ and M_{SiO_2} are the molar masses of the oxides; 291.5 and 60.1 g respectively. Fig. 3(a) also shows the simple linear interpolation of the end member densities (dotted line).

This assumes that there is little change in the structural units involved when they are in combination in the glass. The end member values for V_M used were 55.2 cm^3 $mole^{-1}$ for v-Sb_2O_3 [6] and 27.3 cm^3 $mole^{-1}$ for v-SiO_2. Figs. 3(a) and (b) show some (~2.5–3.0%) negative deviation from the calculated ρ curve and some positive deviation of the V_M values. This could mean that mixing of the Sb and Si polyhedra requires extra free volume. The calculation does not take into account the presence of any Sb^{5+} in the glasses, which would most likely adopt octahedral coordination with ~6% increase in site volume – a minor contribution to the discrepancy.

Density values reported by Datta et al. [4] are also shown in Figs. 3(a) and (b). These values deviate significantly from our results and also the calculated densities but, since these samples were prepared by a sol–gel route, there was possibly some porosity or retained organics in the structure.

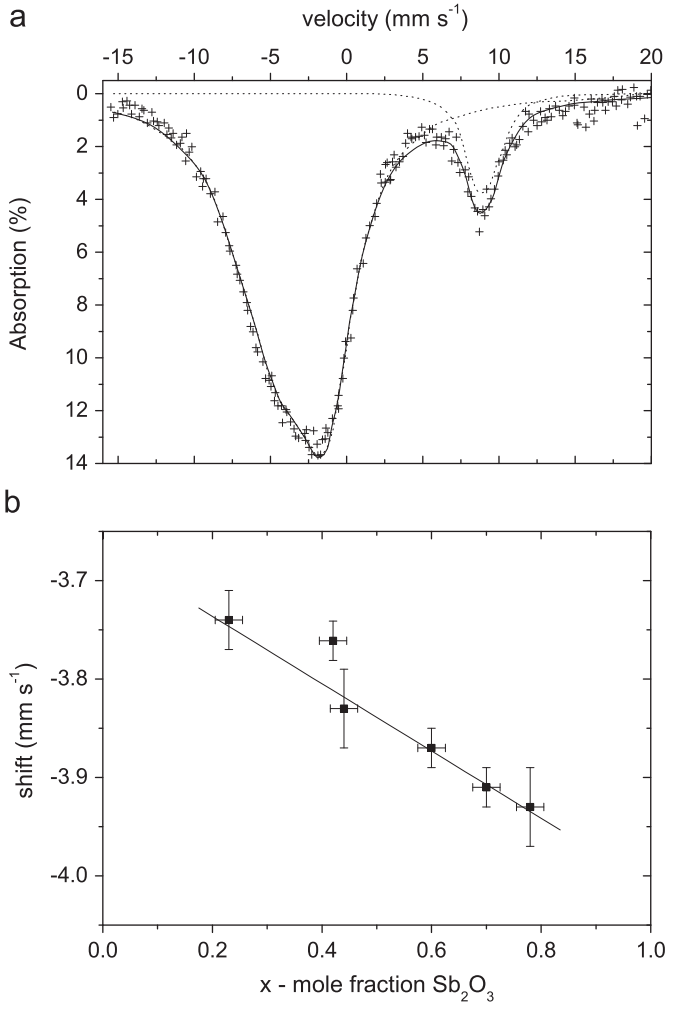

Fig. 4. (a) ^{121}Sb Mössbauer spectrum from the x=0.78 sample of $x$$Sb_2O_3$·(1−$x$)-$SiO_2$. The velocity axis has been corrected to the InSb standard: (+) data; (——) total fit; (· · · · · ·) individual fits and (b) Change in Mössbauer shift, δ, with analysed composition, x, of $x$$Sb_2O_3$·(1−$x$)$SiO_2$.

3.5. Mössbauer

A representative Mössbauer spectrum is shown in Fig. 4(a) for the x=0.78 sample. The peaks in this spectrum arise from Sb^{3+}, with a Mössbauer shift, δ, of ~−3.8 mm s^{-1} and Sb^{5+}, with a δ of ~9 mm s^{-1}. They were fitted with a lineshape consistent with the 7/2↔5/2 transition and the parameters obtained (Mössbauer shift, quadrupole splitting, width and area) are summarised in Table 2. The quadrupole splitting is difficult to discriminate from the width, given the complex lineshape and poor signal-to-noise, particularly for the much smaller Sb^{5+} peak. Hence the errors are large and no systematic change can be discerned. However, the Mössbauer shift for Sb^{3+} showed small, but systematic, changes with composition (Fig. 4(b)), implying that the average Sb environment is changing subtly as the concentration of Sb_2O_3 is increased. A change to more negative values of Mössbauer shift could imply that the ^{121}Sb nucleus is becoming more shielded as x increases (the fractional change in the nuclear radius, $\delta R/R$, on going from the ground state to the excited state is negative for ^{121}Sb), i.e. there is greater s-electron density at the nucleus. This can reflect changes in coordination number, next-nearest neighbour, Sb–O bond length or O–Sb–O bond angle (a consequence of the amount of p_z character in the lone-pair) [20]. We have not taken into account any contribution from the second-order Doppler shift but this may reasonably be expected to be very similar for the various compositions. A large quadrupole splitting, Δ, of ~21 mm s^{-1} is associated with Sb^{3+}, indicative of the highly asymmetric distribution of electric field about the [:SbO_3] trigonal pyramid unit with its lone-pair of electrons. The quadrupole splitting for the more symmetric typical [SbO_6] environment of Sb^{5+} is ~−5 mm s^{-1} but this is difficult to separate from the linewidth contribution and is of doubtful accuracy. These Mössbauer parameters are close in value to those observed for antimony borate glasses [15] where δ values were reported to be ~−3.8 mm s^{-1} for Sb^{3+} and ~8.9 mm s^{-1} for Sb^{5+} whilst Δ ~18 mm s^{-1} was quoted for Sb^{3+}. The closeness of these values to those for valentinite, Sb_2O_3 (δ=−3.32 mm s^{-1}; Δ=18.3 mm s^{-1}) [21] and crystalline Sb_2O_5 (δ=8.54 mm s^{-1}; Δ=−3.72 mm s^{-1}) [22] emphasises the similarities of the Sb environments in the glass and the corresponding crystals. This is in contrast to the Mossbauer parameters of Sb^{3+} and Sb^{5+} in cervantite (Sb_2O_4). In this work the measured values $\delta(Sb^{3+})$=−6.8(3) mm s^{-1}, $\Delta(Sb^{3+})$=18.0(3) mm s^{-1}, $\delta(Sb^{5+})$=9.1(2) mm s^{-1}, $\Delta(Sb^{5+})$=7.3(7) mm s^{-1} for cervantite are in only fair agreement with those of Kajitani [21], $\delta(Sb^{3+})$=−6.02 mm s^{-1}, $\Delta(Sb^{3+})$=15.6 mm s^{-1}, $\delta(Sb^{5+})$=8.85 mm s^{-1}, $\Delta(Sb^{5+})$=−5.1 mm s^{-1} but it is clear that, while the Sb^{3+} and Sb^{5+} environments in the glasses are similar to those in crystalline Sb_2O_3 and Sb_2O_5, respectively, they are different from those in cervantite.

The other values obtained from the fitting are the areas of the two peaks which, if the same f-factors are assumed for the two species, are in the same ratio as their abundances. The change in the percentage of Sb present in the Sb^{5+} state with x is shown in Fig. 5. The data are reasonably well fitted by a straight line of slope 0.12. This contrasts with the corresponding data from antimony borate glasses [15] where a power law fit of $y=25x^{1.7}$ is required (Fig. 5).

3.6. Raman spectroscopy

Fig. 6(a) shows Raman spectra from some of the glass compositions studied. The left-hand side of the figure shows the low frequency region, which is dominated by Sb–O vibrations, whilst the right-hand side, with a 5x expanded y-scale, covers the

Table 2
Mössbauer parameters.

x	Mössbauer parameters for Sb^{3+}				Mössbauer parameters for Sb^{5+}			
	Shift δ ($mm\ s^{-1}$)	Quadrupole splitting Δ ($mm\ s^{-1}$)	Width ($mm\ s^{-1}$)	Area (%)	Shift δ ($mm\ s^{-1}$)	Quadrupole splitting Δ ($mm\ s^{-1}$)	Width ($mm\ s^{-1}$)	Area (%)
0.23	−3.74 (3)	21.6 (3)	4.58 (10)	96.7 (5)	10.3 (4)	−12 (4)	2.5 (11)	3.3 (5)
0.42	−3.76 (2)	19.9 (2)	3.98 (4)	94.8 (5)	9.18 (7)	3 (2)	2.5	5.2 (5)
0.44	−3.83 (4)	21.1 (4)	4.61 (12)	94.4 (5)	9.27 (14)	−4 (2)	2.5	5.6 (5)
0.6	−3.87 (2)	20.8 (2)	4.33 (5)	93.1 (5)	9.04 (6)	−4.9 (14)	2.3 (3)	6.9 (5)
0.7	−3.91 (2)	20.8 (2)	4.36 (5)	91.6 (5)	9.13 (5)	−5.7 (9)	2.1 (2)	8.4 (5)
0.8	−3.93 (4)	21.9 (4)	4.45 (12)	90.1 (5)	9.05 (9)	−5 (3)	3.3 (6)	9.9 (5)

Shifts are referenced to InSb. Numbers in brackets are errors on last significant figures. Where these are missing, the parameter has been fixed.

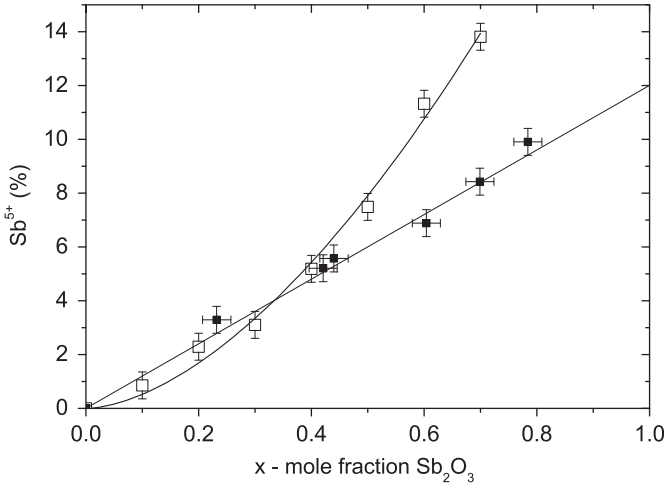

Fig. 5. Percentage of antimony present as Sb^{5+}, derived from ^{121}Sb Mössbauer measurements: (■) data from the $xSb_2O_3 \cdot (1-x)SiO_2$ system, with linear fit; (□) data from the $xSb_2O_3 \cdot (1-x)B_2O_3$ system, with power law fit.

region where the Si–O vibrations dominate (though it should be noted that there are features in this region even in pure v-Sb_2O_3). The feature at $\sim 720\ cm^{-1}$ is associated with non-bridging oxygens (NBO) and the feature at $\sim 950\ cm^{-1}$ is associated with bridging oxygens (BO). The former increases in area as x increases. Fig. 6(b) compares the Raman spectrum from a $xSb_2O_3 \cdot (1-x)SiO_2$ glass ($x=0.43$) with spectra from the two crystalline polymorphs of Sb_2O_3, senarmontite and valentinite. The spectra from the crystalline polymorphs are consistent with those previously reported [23] and there are no significant similarities between the vibrational spectra of the glass and those of the crystals. Terashima et al. [11], in their study of Sb_2O_3–B_2O_3 glasses, assigned a broad signal at $\sim 440\ cm^{-1}$ to bending modes of the [:SbO_3] unit and we similarly assign the intense band at $\sim 410\ cm^{-1}$ in the spectra from the Sb_2O_3–SiO_2 glasses.

3.7. ^{29}Si NMR

A selection of the ^{29}Si MAS NMR spectra obtained from the glasses is shown in Fig. 7. The peaks are generally broad and slightly asymmetric and no spinning sidebands are visible. The degree of asymmetry changes with composition. The main change to the spectrum as x is increased is in the position of the peak maximum, which initially remains fairly constant and then moves steadily to less negative values (more deshielded) as shown in Fig. 8 in comparison with similar plots for the SnO–SiO_2 [24] and PbO–SiO_2 glasses [25]. Here x is replaced by x' from

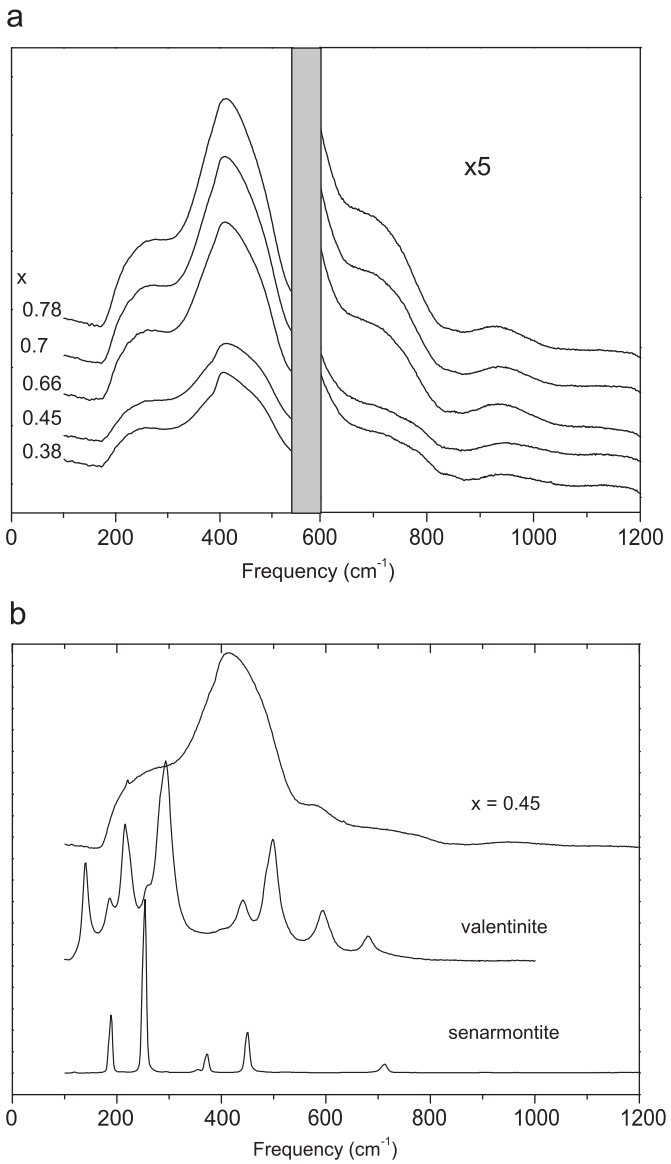

Fig. 6. (a) Comparison of Raman spectra from $xSb_2O_3 \cdot (1-x)SiO_2$ glasses for $x=0.38$, 0.45, 0.66, 0.7, 0.78. The y-axis of the right hand portion of the graph has been expanded by $x5$ and (b) Comparison of the Raman spectrum from one of the $xSb_2O_3 \cdot (1-x)SiO_2$ glasses with $x=0.45$ and spectra from the crystalline polymorphs of Sb_2O_3, valentinite and senarmontite.

$x'Sb_{2/3}O \cdot (1-x')SiO_2$ to allow a consistent basis for comparison and to eliminate the effect of different charges on the cations. It can be seen that the ^{29}Si peak position remains unchanged up to

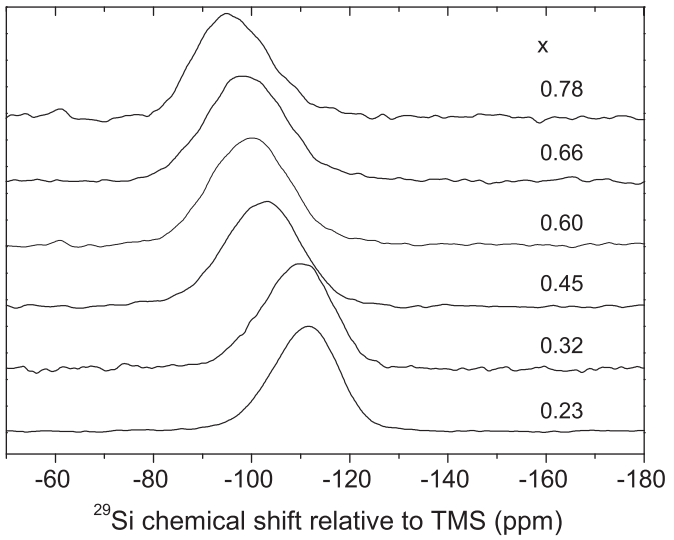

Fig. 7. ^{29}Si MAS NMR spectra from $x Sb_2O_3 \cdot (1-x)SiO_2$ glasses with $x=0.23$, 0.32, 0.45, 0.60, 0.66, 0.78.

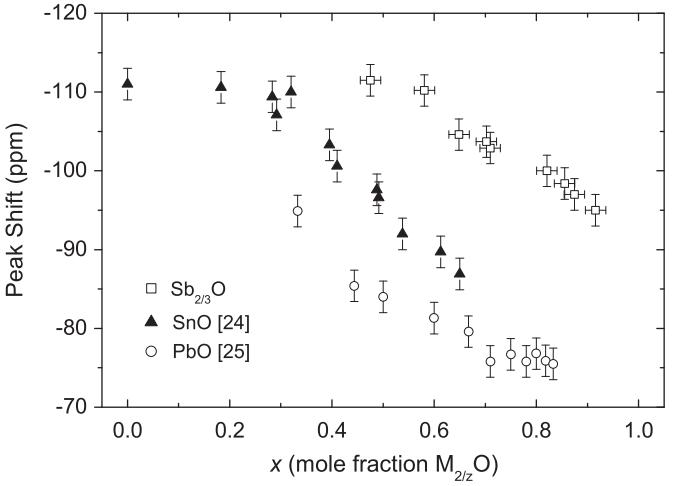

Fig. 8. Change in ^{29}Si *peak* shift with composition, x, in $xM_{2/z}O \cdot (1-x)SiO_2$, where z is the charge on the cation and M=Pb (○), Sn (▲), Sb (□).

$x'=0.48$ ($x=0.23$), implying that either there is no mixing of the two networks or that there is little difference between Si–O–Sb and Si–O–Si linkages.

The spectra were fitted with Gaussian lineshapes. However, the absence of detail in the spectrum lineshape means that an unambiguous fit cannot be obtained and various constraints need to be applied. An example of the fitting is shown in Fig. 9 for the $x=0.23$ sample. The peak in the spectrum is asymmetric and therefore a single Gaussian is insufficient to fit the spectrum. Fig. 9(a) shows a 2-peak fit but, whilst this is a satisfactory (and unconstrained) fit, the intensities of the 2 peaks are inconsistent with this concentration of Sb_2O_3. If Sb_2O_3 were considered to be a conventional modifier oxide, and a binary distribution of Q^n species were a good description of the glass structure, then no Q^4 species should be present at $x=0.23$ because each molecule of Sb_2O_3 would produce 6 non-bridging oxygens (NBO) giving the number of bridging oxygens (BO) per silicon as 1.1 – i.e. predominantly Q^1 and some Q^2. The chemical shifts of the peaks in the 2-peak fit in Fig. 9(a) are -112 ± 1 and -104 ± 1 ppm, which are typical of Q^4 and Q^3, respectively. Even if Sb_2O_3 were considered to produce only 2 NBO per molecule, the NBO/Si ratio would be 2.3 – i.e. a mixture of Q^3 and Q^2. Moreover, the line

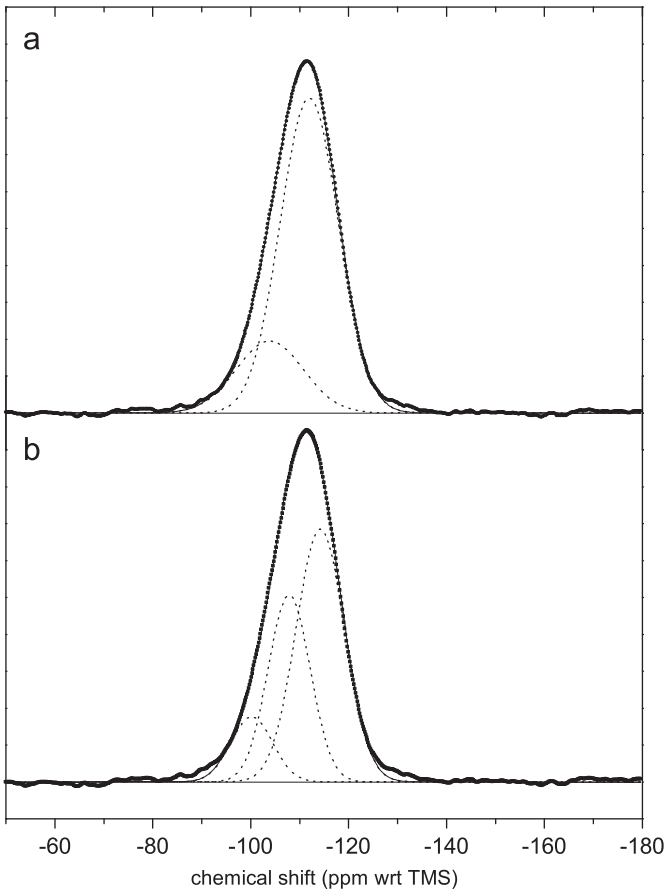

Fig. 9. ^{29}Si MAS NMR spectrum of $x=0.23$ glass: (a) 2-peak fit and (b) 3-peak fit. Points are data, dotted lines are individual fits and the solid line is the overall fit.

widths of the peaks are inconsistent with previous NMR studies of silicates which show greater widths for the more constrained Q^4 species. Thus a 3-peak fit of the spectrum was attempted. This could only be achieved by assuming a *statistical* distribution of Q^n species in which the abundances of species as a function of x are given by the following equations:

$$\%Q^4 = 100 \times \left[\frac{2-3x}{2-2x}\right]^4$$

$$\%Q^3 = 100 \times 4 \times \left[\frac{x}{2-2x}\right]\left[\frac{2-3x}{2-2x}\right]^3$$

$$\%Q^2 = 100 \times 6 \times \left[\frac{x}{2-2x}\right]^2\left[\frac{2-3x}{2-2x}\right]^2$$

$$\%Q^1 = 100 \times 4 \times \left[\frac{x}{2-2x}\right]^3\left[\frac{2-3x}{2-2x}\right]$$

$$\%Q^0 = 100 \times \left[\frac{x}{2-2x}\right]^4$$

The areas of the fitted peaks were then constrained to be in the ratio predicted by the statistical model and, whilst the other parameters (chemical shift, halfwidth) could be refined, this is predominantly simulation rather than fit. The results of this are shown in Fig. 9(b), where the spectrum from $x=0.23$ is accurately simulated by three peaks from Q^4, Q^3 and Q^2 (Q^1 and Q^0 can be neglected at this composition). Fig. 10 shows a 4-peak fit to the spectrum from the $x=0.31$ sample. Here we chose not only to fix the Q^3 intensity but also to fix the halfwidths of the other three peaks. Again an acceptable simulation/fit of the spectrum was achieved. Beyond $x=0.38$, the statistical model is less successful at simulating the spectra and further fitting used only the

constraint that the halfwidths should remain at the values determined for the lower values of x. Fig. 11 shows a 5-peak fit to the spectrum from the $x=0.66$ sample. Fig. 12 shows how the abundances of the various Q^n species change with composition, x, in comparison with the changes predicted on the basis of applying the statistical model to the $x Sb_2O_3 \cdot (1-x)SiO_2$ system assuming that 2 "NBO" are formed for each Sb_2O_3 molecule. In the context of this system, "NBO" are Si–O–Sb oxygen links where there will be significant covalence in the bonding (*v.i.*).

4. Discussion

The Mössbauer parameters obtained for the dominant Sb^{3+} species in the glasses are typical of the trigonal pyramid [:SbO_3] units produced by the presence of the lone-pair of electrons in a hybridised $s^x p^y$ orbital. This result is consistent with the EXAFS data of Ellison and Sen [18] who report a Sb–O coordination of 3 and Sb–O distance of ~1.95–1.97 Å, which are close to the values observed for senarmontite where the O–Sb–O angle is close to tetrahedral. The low coordination number for Sb–O indicates that it could easily take part in a glass network and we need to understand its effect on the silicate units.

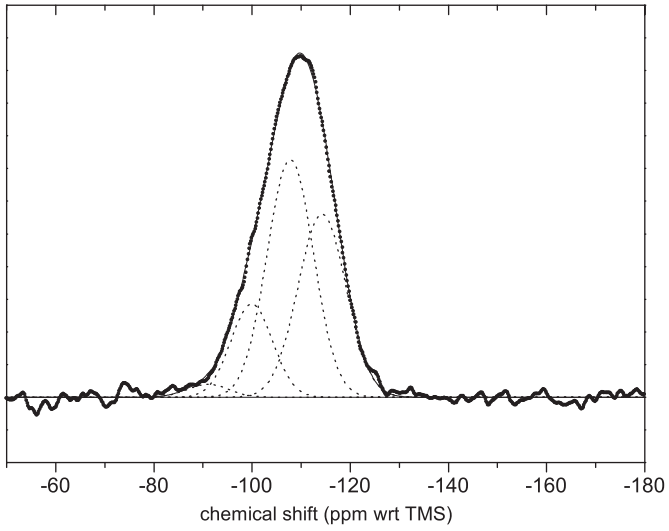

Fig. 10. ^{29}Si MAS NMR spectrum of $x=0.31$ glass: 4-peak fit. Points are data, dotted lines are individual fits and the solid line is the overall fit.

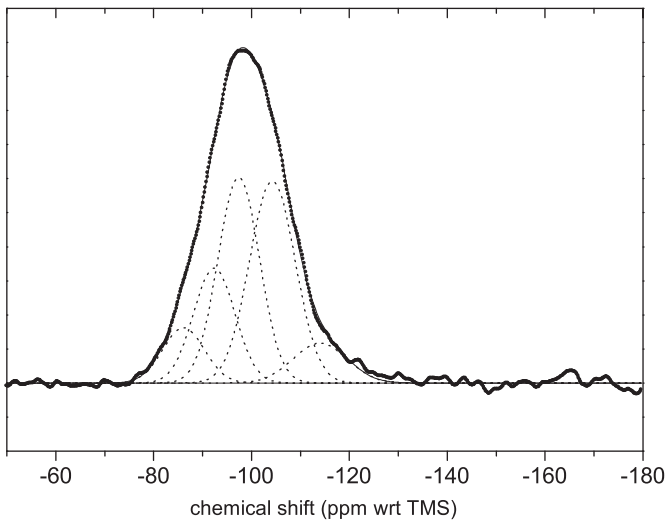

Fig. 11. ^{29}Si MAS NMR spectrum of $x=0.66$ glass: 5-peak fit. Points are data, dotted lines are individual fits and the solid line is the overall fit.

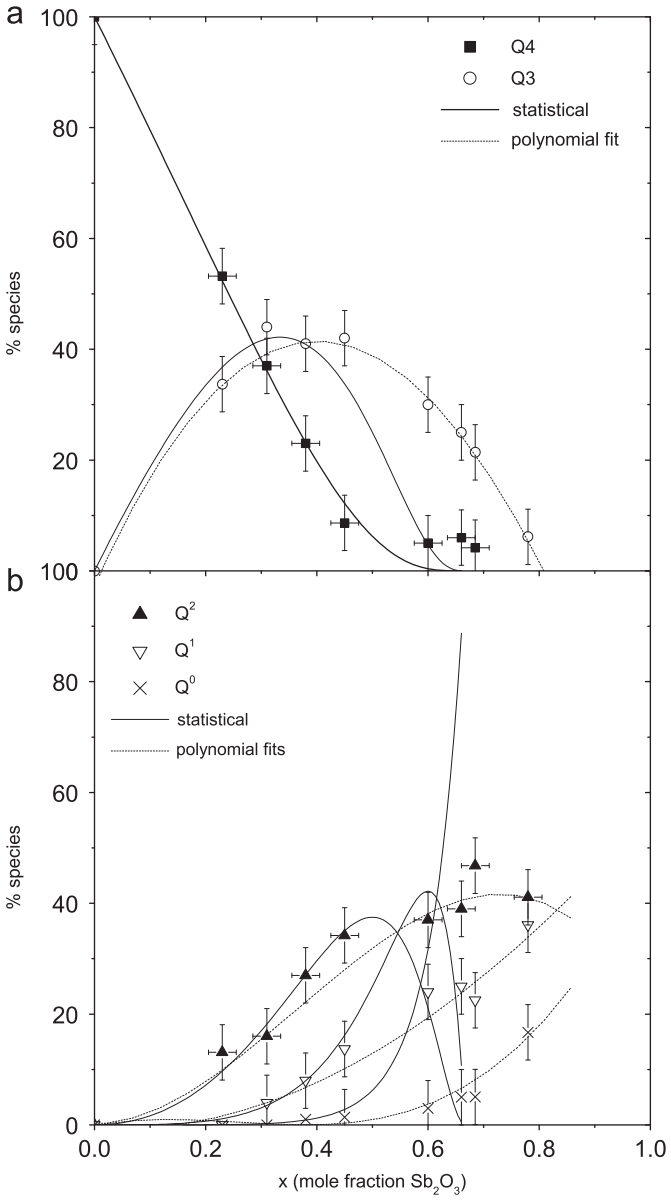

Fig. 12. Change in abundance of the various Q^n species as a function of analysed composition, x, in $x Sb_2O_3 \cdot (1-x)SiO_2$: (a) Q^4 (■) and Q^3 (○); (b) Q^2 (▲), Q^1 (▽) and Q^0 (×). Solid lines are the dependencies predicted by the statistical distribution assuming only 2 "NBO" per molecule of Sb_2O_3. Dotted lines are polynomial fits to the data points.

The NMR results give a Q^n distribution, which is very different from that associated with conventional modifier oxides but we can use the same approach to try to understand how the [:SbO_3] units are bonded into the silicate network. The x parameter used in the equations for a statistical distribution (*v.s.*) are based on the general formula $x R_2O \cdot (1-x)SiO_2$ i.e. for an alkali, R_2O (or alkaline earth, RO) silicate, where every unit of cation charge translates into a NBO. In the case of Sb_2O_3, there is three times as much nominal charge per oxide unit and therefore one molecule of Sb_2O_3 should yield 6 NBO. This would result in all Si becoming isolated Q^0 species at $x=0.4$ which is not consistent with the Q^n population determined from NMR. When referring to conventional modifiers, it is usual to expect glass formation to become difficult when there are more than 2 NBO per Si – i.e. at $x=0.25$.

This is plainly not the case and suggests that Sb_2O_3 should not be treated as a conventional modifier. Since Sb_2O_3 is known to be itself capable of glass formation, albeit with difficulty, this is not surprising. We must therefore think in terms of Si–O–Sb bonds rather than NBO but we will retain this convenient, though inaccurate, label during our discussion.

We also need to consider the effect of the existence of Sb–O–Sb links in the glass network. This could begin to occur when the number of Si–O–Si links falls below a certain number, or such links could be present even at low concentrations. Models for the latter can be devised where the antimony-oxygen structural units, containing different Sb–O–Sb links, are altered so as to modify the number of NBO formed per Sb_2O_3 unit. The resulting distribution of these NBO amongst the Si atoms will result in Q^n distributions which can be calculated using the statistical formulae above and compared with those determined experimentally. The possible structural units which might enter the glass are summarised in Table 3, along with the number of NBO which this would generate for each molecule of Sb_2O_3. The first unit is the isolated [:SbO_3] pyramid, thus there are 6 "NBO" per Sb_2O_3 molecule. The second unit comprises two [:SbO_3] pyramids which share a corner. This unit can thus form 4 "NBO" per Sb_2O_3 molecule. The third unit could be two [:SbO_3] pyramids which share an edge and thus provide 2 "NBO" per Sb_2O_3 molecule. The last unit would then have two of the previous units joined at one corner and thus giving 1 "NBO" per Sb_2O_3 molecule. However, edge-sharing does not occur to any significant extent in networks and a more likely description of the 2 "NBO" and 1 "NBO" units is that they consist of 8-membered rings (4 [:SbO_3] pyramids joined at corners) – single in the case of the 2 "NBO" unit (Fig. 13(a)) and fused in threes in the case of the 1 "NBO" (Fig. 13(b)). The 2 "NBO" and 1 "NBO" units resemble fragments of the valentinite structure [26] (Fig. 13(c)). The compositions of the glasses are then expressed in terms of the mole fractions of Sb_2O_3 when described by these structural units and assuming that they are the sole species present. The experimental Q^n distributions are then plotted against mole fraction Sb_2O_3 in Figs. 14(a)–(e) and compared with the lines predicted by the statistical model for the different structural units in Table 3. It is apparent from these plots that the Q^n distributions are best described by the introduction of 2 "NBO" units into the structure up to the $x\sim0.5$ composition and by introduction of 1 "NBO" units beyond this.

Possible phase separation of the glass into SiO_2 and Sb_2O_3-rich regions must also be considered as an explanation of the Q^n distributions. There is no visible evidence of phase separation in samples in the current study, with the exception of the $x=0.3$ sample. Since the separation here was macroscopic – regions several mm in extent – this is thought to be a mixing problem. Only the regions with composition $x=0.31$ were used in measurements. Ellison and Sen [18] comment on the invariance with concentration of the Sb–O distance in the various glass systems which they studied, though there was some dependence on the network oxide with which Sb_2O_3 was combined. From the limited next-nearest neighbour information, which they could obtain from the Sb *K*-edge EXAFS of arsenate and germanate glasses, they state that "antimony mixes very homogeneously with other glass forming constituents". The single, and smoothly changing with x, T_g values which we obtain for these glasses also indicate single phase samples. The isomer shifts from the ^{121}Sb Mössbauer measurements also vary smoothly with composition and there is no evidence of changing peak width which would occur if regions of different environments were present. Datta et al. [4] ascribe some of the electrical phenomena, which they observed to layers of varying antimony concentration in their sample. Since these samples were made by a sol–gel route and have anomalously low densities, they cannot reasonably be compared with the glasses in this study.

It is notable that the Q^4 chemical shift, which results from these fits is ~ -114 ppm. This is somewhat larger than the -109 to -112 ppm usually reported for Q^4 with all Q^4 next-nearest neighbours and could indicate a shortening of the Si–O bond or an

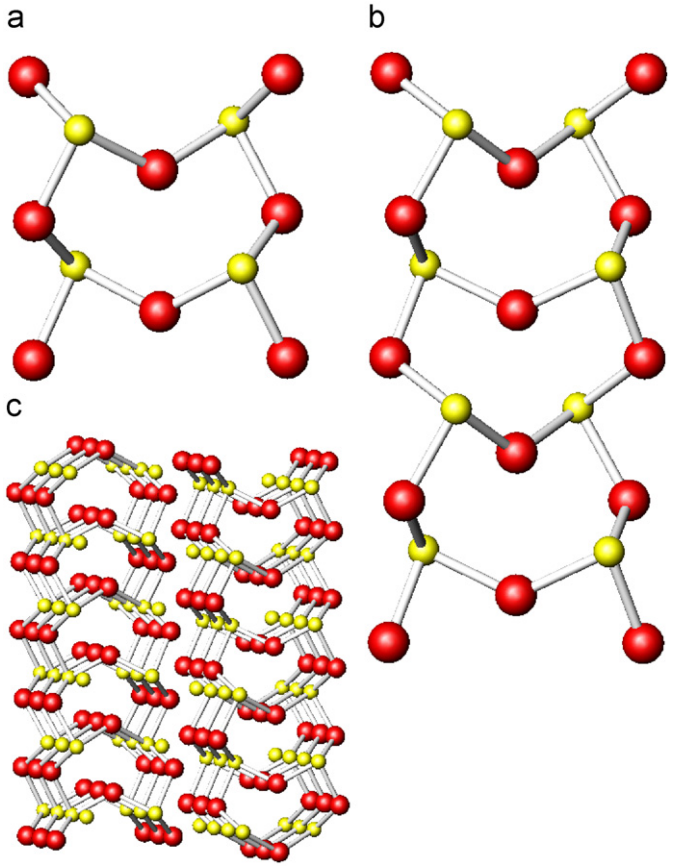

Fig. 13. Structural units for (a) 2 "NBO" per Sb_2O_3 model; (b) 1 "NBO" per Sb_2O_3 model; and (c) valentinite (drawn using Atoms V6.2)

Table 3
Structural units possibly formed by Sb_2O_3 in the glass; their mole fraction; and the number of NBO (Si–O–Sb links) which would be associated with them.

Structural unit	Description	Mole fraction in terms of x	NBO/Sb_2O_3
Sb^{3+}	Isolated [:SbO_3] pyramids	$3x/(1+2x)$	6
$(O-)_2Sb-O-Sb(-O)_2$	2 pyramids joined at one corner	$2x/(1+x)$	4
$O-Sb=O_2=Sb-O$	2 pyramids joined at one edge	x	2
OR $[O-Sb<O_{2/2}]_4$	4 pyramids joined in a ring		
$O-Sb=O_2=Sb-O-Sb=O_2=Sb-O$	2 of the above units connected	$x/(2-x)$	1
OR $[O-Sb<O_{2/2}]_4[SbO_{3/2}]_4$	3 fused rings		

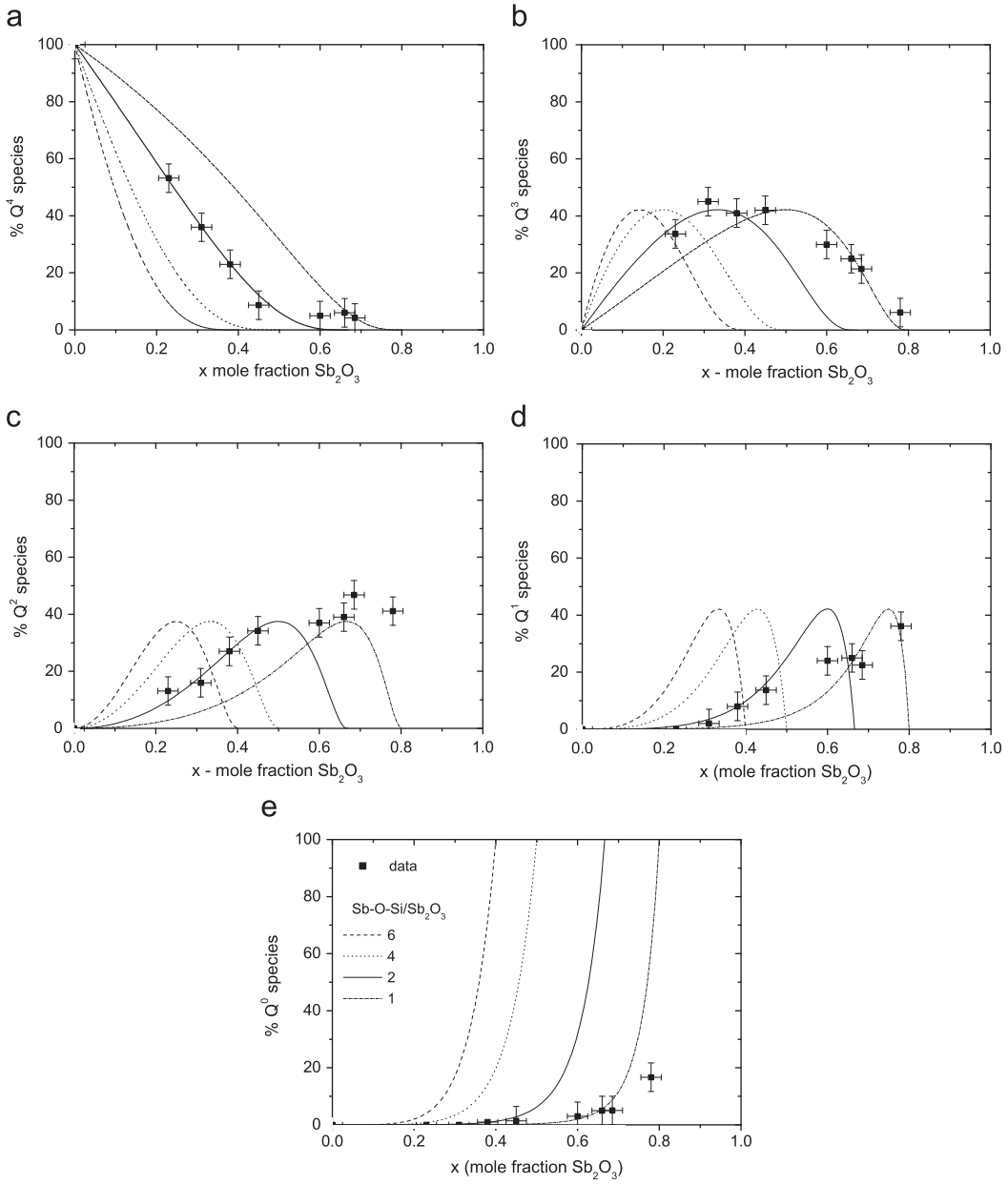

Fig. 14. Q^n abundances plotted against mole fraction of the effective structural units listed in Table 2. The lines are the values predicted by the statistical model for different numbers of NBO per Sb_2O_3 molecule: (– – –) 6 NBO; (· · · · · ·) 4 NBO; (—) 2 NBO; and (–·–·) 1 NBO.

increase in the mean Si–O–X bond angle. Various empirical relationships have been derived for the dependence of chemical shift, δ, on bond length in crystalline silicates [27]. These are mostly linear – of the form $\delta = a(d_{Si-O}) - b$, where a and b are constants obtained for particular series of related silicates and which are useful predictors within their parent series but less good outside. A universal formula, which is only an approximation for most series, is $\delta = 999(d_{Si-O}) - 1709$ [27]. A δ value of -114 ppm would then correspond to a Si–O bond length of 1.5966 Å. This can be compared to a value of 1.61–1.62 Å in ν-SiO_2 and a value of 1.6088 Å in a $0.168SnO \cdot 0.832SiO_2$ glass [28] though these values correspond to the centres of distributions which range from ~1.5 to ~1.8 Å at their base. The mean Si–O bond length determined by diffraction measurements on binary silicate glasses generally increases as the second component (X) is added. This is a consequence of the increase in the Si–O(Si) bond length whilst the Si–O(X) bond length shortens (for X modifier). Similar empirical linear relationships exist between δ and some trigonometric function of the mean Si–O–X bond angle but these are even more series specific[27].

5. Conclusions

Sb_2O_3 can be incorporated into SiO_2 to give single phase glasses over at least the range $0.1 \le x \le 0.8$ in $xSb_2O_3 \cdot (1-x)SiO_2$. Physical parameters such as density, molar volume, glass transition temperature change smoothly with x, as also do the fraction of Sb^{5+} formed and the Mössbauer isomer shift. The change in the Q^n population with x can be related to the incorporation of Sb_2O_3 structural fragments in the glasses. Below $x \sim 0.5$, the fragments are probably ($Sb_4O_4O_{4/2}$) rings with 4 NBO ($O_{4/2}$), whilst above $x \sim 0.5$, the fragments are composed of 3 rings fused together to give ($Sb_8O_{10}O_{4/2}$) units with 4 NBO. The

existence of such units should be evidenced in diffraction studies by the presence of characteristic Sb···Sb distances at concentrations where they should not statistically exist.

Acknowledgment

EPSRC are thanked for the provision of a studentship (RGO) and for partial funding of the NMR equipment at Warwick.

References

[1] J. Minelly, A. Ellison, Opt. Fiber Technol. 8 (2002) 123–138.
[2] M. Shimizu, Y. Ohmori, J. Lightwave Technol. LT-5 (1987) 763.
[3] D. Chakravorty, D. Kumar, G. Sastry, J. Phys. D: Appl. Phys. 12 (1979).
[4] A. Datta, A.K. Giri, D. Chakravorty, J. Phys.: Condens. Matter 4 (1992) 1783–1790.
[5] W.H. Zachariasen, J. Am. Chem. Soc. 54 (1932) 3841–3851.
[6] R.G. Orman, S. Feller, A.C. Hannon, D. Holland 2010, to be submitted.
[7] J.F. Bednarik, J.A. Neely, Glastechn. Ber. 55 (1982) 126–129.
[8] J.F. Bednarik, J.A. Neely, Phys. Chem. Glasses 23 (1982) 204–205.
[9] H. Hasegawa, M. Stone, M. Imaoka, Phys. Chem. Glasses 19 (1978) 28–33.
[10] H. Masuda, Y. Ohta, K. Morinaga, Nippon Kinzoku Gakkaishi 59 (1995) 31–36.
[11] K. Terashima, T. Hashimoto, T. Uchino, S.-H. Kim, T. Yoko, J. Ceram. Soc. Japan 104 (1996) 1008.
[12] J.A. Johnson, D. Holland, J. Bland, C.E. Johnson, M.F. Thomas, J. Phys.: Condens. Matter 15 (2003) 755–764.
[13] M. Imaoka, H. Hasegawa, S. Shindo, Yogyo-Kyokai-Shi 84 (1969) 263.
[14] N. Mochida, K. Takahashi, Yogyo-Kyokai-Shi 84 (1976) 413.
[15] D. Holland, A.C. Hannon, M.E. Smith, C.E. Johnson, M.F. Thomas, A.M. Beesley, Solid State NMR 26 (2004) 172–179.
[16] R.E. Youngman, S. Sen, L.K. Cornelius, A. Ellison, Phys. Chem. Glasses 44 (2003) 69.
[17] S. Chatlani, J.E. Shelby, Phys. Chem. Glasses: Eur. J. Glass Sci. Technol. B 47 (2006) 288–293.
[18] A.J.G. Ellison, S. Sen, Phys. Rev. B 67 (2003) 052203.
[19] R.G. Orman, D. Holland, J. Solid State Chem. 180 (2007) 2587–2596.
[20] N.N. Greenwood, T.C. Gibb, in: Mossbauer Spectroscopy., Chapman & Hall, London, 1971.
[21] Y. Kajitani, M. Takahashi, M. Takeda, Int. J. Inorg. Mater. 3 (2001) 337–340.
[22] V.M. Jansen, J. Pebler, K. Dehnicke, Z. Anorg. Allg. Chem. 496 (1982) 120–126.
[23] E.I. Voit, A.E. Panasenko, L.A. Zemnukhova, J. Struct. Chem. 50 (2009) 60–66.
[24] D. Holland, A.P. Howes, R. Dupree, J.A. Johnson, C.E. Johnson, J. Phys.:Condens. Matter 15 (2003) S2457–S2472.
[25] S. Feller, G. Lodden, A. Riley, et al., J. Non-Cryst. Solids 356 (2010) 304–313.
[26] C. Svensson, Acta Crystallogr. B 30 (1974) 458–461.
[27] K.J.D. Mackenzie, M.E. Smith, in: Multinuclear Solid-State NMR of Inorganic Materials, Pergamon, 2002.
[28] J.F. Bent, A.C. Hannon, D. Holland, M.M.A. Karim, J. Non-Cryst. Solids 232&234 (1998) 300–308.